

## Porous organic cages for sulfur hexafluoride separation

Hasell, T., Miklitz, M., Stephenson, A., Little, M. A., Chong, S. Y., Clowes, R., Chen, L., Holden, D., Tribello, G., Jelfs, K. E., & Cooper, A. I. (2016). Porous organic cages for sulfur hexafluoride separation. *Journal of the American Chemical Society*. <https://doi.org/10.1021/jacs.5b11797>

**Published in:**

Journal of the American Chemical Society

**Document Version:**

Peer reviewed version

**Queen's University Belfast - Research Portal:**

[Link to publication record in Queen's University Belfast Research Portal](#)

**Publisher rights**

This document is the Accepted Manuscript version of a Published Work that appeared in final form in *Journal of the American Chemical Society*, copyright © 2016 American Chemical Society after peer review and technical editing by the publisher. To access the final edited and published work see <http://pubs.acs.org/doi/abs/10.1021/jacs.5b11797>

**General rights**

Copyright for the publications made accessible via the Queen's University Belfast Research Portal is retained by the author(s) and / or other copyright owners and it is a condition of accessing these publications that users recognise and abide by the legal requirements associated with these rights.

**Take down policy**

The Research Portal is Queen's institutional repository that provides access to Queen's research output. Every effort has been made to ensure that content in the Research Portal does not infringe any person's rights, or applicable UK laws. If you discover content in the Research Portal that you believe breaches copyright or violates any law, please contact [openaccess@qub.ac.uk](mailto:openaccess@qub.ac.uk).

# Porous organic cages for sulfur hexafluoride separation

Tom Hasell, Marcin Miklitz,<sup>‡</sup> Andrew Stephenson, Marc A. Little, Samantha Y. Chong, Rob Clowes, Linjiang Chen, Daniel Holden, Gareth A. Tribello,<sup>†</sup> Kim E. Jelfs,<sup>‡</sup> and Andrew I. Cooper\*

Department of Chemistry and Centre for Materials Discovery, University of Liverpool, Crown St., Liverpool L69 7ZD, UK.

<sup>‡</sup> Department of Chemistry, Imperial College London, South Kensington, London, SW7 2AZ, U.K.

<sup>†</sup> Atomistic Simulation Centre, Department of Physics and Astronomy, Queen's University Belfast, University Road, Belfast, BT7 1NN, U.K.

**KEYWORDS** Porous organic cages; microporous; SF<sub>6</sub>; gas separation, crystal engineering.

---

**ABSTRACT:** A series of porous organic cages is examined for the selective adsorption of sulphur hexafluoride (SF<sub>6</sub>) over nitrogen. Despite lacking any metal sites, a porous cage, **CC3**, shows the highest SF<sub>6</sub>/N<sub>2</sub> selectivity reported for any material at ambient temperature and pressure, which translates to real separations in a gas breakthrough column. The SF<sub>6</sub> uptake of these materials is considerably higher than would be expected from the static pore structures. The location of SF<sub>6</sub> within these materials is elucidated by x-ray crystallography, and it is shown that cooperative diffusion and structural rearrangements in these molecular crystals can rationalize their superior SF<sub>6</sub>/N<sub>2</sub> selectivity.

---

## INTRODUCTION

Sulfur hexafluoride (SF<sub>6</sub>) is a much more potent greenhouse gas than CO<sub>2</sub>,<sup>1,2</sup> with an estimated atmospheric lifetime of 800–3200 years.<sup>1</sup> The Intergovernmental Panel on Climate Change found SF<sub>6</sub> to be the most potent greenhouse gas that it evaluated, with a global warming potential 23,900 times higher than CO<sub>2</sub>.<sup>3</sup> Nonetheless, SF<sub>6</sub> has valuable and widespread industrial uses. For example, SF<sub>6</sub> or SF<sub>6</sub>/N<sub>2</sub> mixtures are often used to insulate electrical equipment.<sup>2,4</sup> SF<sub>6</sub> is also a good thermo-acoustic insulator for windows, a contrast agent in medical applications, and a plasma etchant in the semiconductor industry.<sup>5</sup> There is much current interest in finding effective materials for the separation of SF<sub>6</sub> from gas mixtures to prevent its release into the atmosphere and to allow economically viable capture and re-use.<sup>6</sup> Pressure swing adsorption / desorption processes using a suitable porous material offer considerable energy savings over liquefaction, but this requires high selectivity for SF<sub>6</sub> adsorption over N<sub>2</sub> adsorption.<sup>7</sup> Various porous solids have been tested for SF<sub>6</sub> adsorption or separation<sup>8</sup> such as carbons,<sup>9,10</sup> zeolites,<sup>11–13</sup> metal-organic frameworks (MOFs),<sup>5,6</sup> and pillared clays.<sup>14</sup> Until now, the most selective of these materials have been zeolite 13X<sup>12</sup> and a series of isostructural MOFs with a high density of unsaturated metal sites.<sup>6</sup> The success of these materials was attributed to their pore diameters (10 and 11 Å, respectively), which were identified by Monte Carlo simulations as close to ideal.

All microporous solids tested for SF<sub>6</sub> separation so far have been insoluble, extended networks or macromolecules. Nitschke *et al* demonstrated that a metal-organic capsule could capture and release SF<sub>6</sub> in solution<sup>27</sup>, but such molecular separation of SF<sub>6</sub> by a cage molecule has not yet been shown in the

gas phase. However, there is also growing interest in porous molecular cages.<sup>15–26</sup> These cages contain an internal void that is accessible via well-defined windows, and the rigid structure of the cages prevents collapse, thus providing porosity for guest molecules. Porous organic cages have been synthesized from imines,<sup>15–17</sup> boronic esters,<sup>28</sup> and by direct carbon-carbon bond forming reactions.<sup>29</sup> Apparent Brunauer–Emmett–Teller (BET) surface areas for nitrogen as high as 3758 m<sup>2</sup> g<sup>−1</sup> have been achieved.<sup>30</sup> Since these cages are discrete molecules, as opposed to frameworks, they are soluble in common organic solvents and can be processed into support materials and precipitated or crystallized into the solid state as required. We previously reported a class of [4+6] cycloimine cage compounds that show gas uptakes and physicochemical stabilities that are remarkable for molecular organic crystals.<sup>31–33</sup> The gas sorption properties of these cages depends both on their molecular structure, and on their crystal packing, and many of these cages can exist as multiple polymorphs.<sup>31,34,35</sup> These cages are excellent candidates for the molecular separation of noble gases,<sup>36</sup> chiral molecules,<sup>36</sup> and hydrocarbon isomers.<sup>37–39b</sup> In this study, a series of these organic cages (Fig. 1) was investigated for their potential in the separation of SF<sub>6</sub>. One cage, **CC3**, shows remarkably high SF<sub>6</sub> selectivity, and this is related to the flexible nature of the molecular cage crystal.

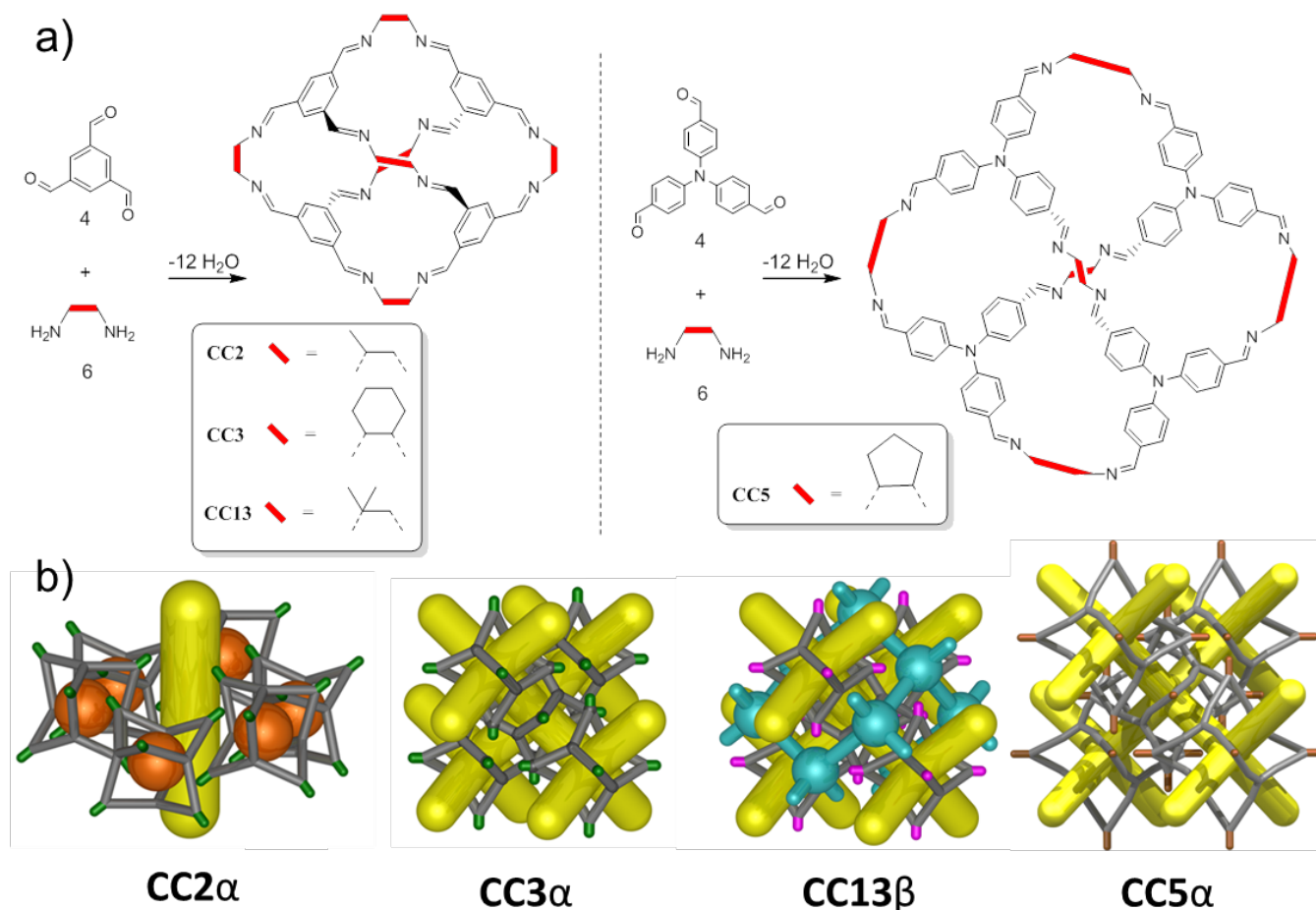


**Figure 1.** a) Synthesis and structure of cages **CC1**, **CC2**, **CC5**, and **CC13**. b) Simplified structural representations of the packing and porosity of these cages as derived from single crystal structures. **CC2 $\alpha$**  exhibits one dimensional pore channels (yellow) in addition to internal cage cavities (orange), which may also be accessible depending on the size of the guest. **CC3 $\alpha$**  has a 3D diamondoid pore network (yellow). **CC13 $\beta$**  packs with the same diamondoid pore network as **CC3 $\alpha$**  (running through the inside of the cages, shown in yellow), but with an additional, narrower interpenetrating diamondoid pore network between the cages (cyan). **CC5 $\alpha$**  packs in the same window-to-window fashion, but the cages and hence the pore channels (yellow) are larger.

## METHODS

**Materials and synthesis:** 1,3,5-Triformylbenzene (TFB) was purchased from Manchester Organics, UK and used as received. 2-Methyl-1,2-propanediamine was purchased from TCI Europe and used as received. All other chemicals were purchased from Sigma-Aldrich and used as received. All cages were synthesized as described previously.<sup>31,33,40,41</sup>

**Gas Sorption Analysis:** Powder samples were degassed off-line at 100 °C for 15 h under dynamic vacuum (10-5 bar) before analysis, followed by degassing on the analysis port under vacuum, also at 100 °C. Isotherms were measured using a micromeritics 3flex surface characterisation analyser, equipped with a Cold-Edge technologies liquid helium cryostat chiller unit for temperature control.

**Single crystal diffraction data:** Evacuated prism shaped single crystals of **CC3 $\alpha$**  were exposed to dry SF<sub>6</sub> at 1 bar pressure. The crystals of were transferred to a sample vial and after 28 hour a single crystal data collection was recorded.

Single crystal X-ray data for **CC3-S'·(SF<sub>6</sub>)<sub>2.5</sub>·(H<sub>2</sub>O)<sub>3</sub>** was measured at beamline I19, Diamond Light Source, Didcot, UK

using silicon double crystal monochromated synchrotron radiation ( $\lambda = 0.6889$  Å, Kappa 4-circle goniometer, Rigaku Saturn724+ detector).<sup>42</sup> Empirical absorption corrections, using equivalent reflections, were applied by the program SADABS.<sup>43</sup> The structure was solved by SHELXD,<sup>44</sup> and refined by full-matrix least squares on  $|F|^2$  by SHELXL,<sup>44</sup> interfaced through the programme OLEX2.<sup>45</sup> Absolute configuration was determined using *a priori* knowledge of the cage chirality. For full refinement details, see SI. Supplementary single crystal XRD data, including structure factors, is available free of charge from the Cambridge Crystallographic Data Centre (CCDC) via [www.ccdc.cam.ac.uk/data\\_request/cif](http://www.ccdc.cam.ac.uk/data_request/cif).

Crystal data for **CC3-S'·(SF<sub>6</sub>)<sub>2.5</sub>·(H<sub>2</sub>O)<sub>3</sub>**, CCDC number CCDC 1437443: Formula C<sub>144</sub>H<sub>174</sub>F<sub>15</sub>N<sub>24</sub>O<sub>3</sub>S<sub>2.5</sub>;  $M = 2654.40$  g·mol<sup>-1</sup>; triclinic space group *P*1, colourless prism shaped crystal;  $a = 17.385(5)$ ,  $b = 17.425(6)$ ,  $c = 17.479(6)$  Å;  $\alpha = 60.384(3)$ ,  $\beta = 60.308(3)$ ,  $\gamma = 60.168(3)^\circ$ ;  $V = 3768(2)$  Å<sup>3</sup>;  $\rho = 1.170$  g·cm<sup>-3</sup>;  $\mu = 0.108$  mm<sup>-1</sup>;  $F(000) = 1405$ ; crystal size =  $0.13 \times 0.07 \times 0.07$  mm<sup>3</sup>;  $T = 100(0)$  K; 52288 reflections measured ( $1.376 < \theta < 25.503^\circ$ ), 28131 unique ( $R_{\text{int}} = 0.0448$ ), 22028 ( $I > 2\sigma(I)$ );  $R_1 = 0.0894$  for observed and  $R_1 = 0.1091$  for all reflections;  $wR_2 = 0.2549$  for all reflections; max/min difference electron

density = 0.801 and  $-0.923 \text{ e}^{-\text{\AA}^{-3}}$ ; data/restraints/parameters = 28131/363/1786; GOF = 1.037. Flack parameter 0.14(4). The structure was refined with the TWINLAW [100 001 010] and BASF refined to 0.227(2).

**Laboratory X-ray powder diffraction:** Powder X-ray diffraction (PXRD) data were collected in transmission mode on loose powder samples held on thin Mylar film in aluminium well plates on a Panalytical X'Pert PRO MPD equipped with a high throughput screening (HTS) XYZ stage, X-ray focusing mirror and PIXcel detector, using Cu K $\alpha$  radiation. Data were measured over the range 4–50° in  $\sim 0.013^\circ$  steps over 60 minutes.

**In situ PXRD gas-loading:** *In situ* powder diffraction data under an SF<sub>6</sub> atmosphere were collected at beamline I11 at Diamond Light Source using the low pressure capillary gas cell.<sup>46</sup> A finely ground sample of **CC13 $\beta$**  was packed in a 0.7 mm diameter borosilicate capillary and mounted on the low-pressure capillary gas cell. Samples were activated by heating to 350 K using an Oxford Cryostream Plus under dynamic vacuum (approximately  $10^{-5}$  bar). Data were collected using the Mythen-II position sensitive detector (PSD)<sup>46</sup> at 230 K. An initial powder diffraction profile of guest-free **CC13 $\beta$**  was collected under dynamic vacuum. The sample was rocked through  $\pm 15^\circ$  in  $\theta$  to improve powder averaging. Gas was dosed into the system, initially to 2.7 bar and then 3 bar. Samples were allowed to equilibrate at both pressures for approximately of 45 minutes after gas was dosed into the cell. PXRD data were collected during this time to monitor equilibration. The sample was then evacuated at 373 K under dynamic vacuum and the powder profile collected to confirm removal of the guest from the pore structure.

**Metadynamics simulations:** A 100 ns well-tempered metadynamics simulation was performed with DL\_POLY2.20<sup>47</sup> and PLUMED2.<sup>48</sup> The OPLS-AA force field parameters,<sup>49</sup> and the Leapfrog Verlet algorithm<sup>50</sup> with a timestep of 0.5 fs was used. The Nose-Hoover thermostat<sup>51</sup> was used to keep the temperature fixed at 300 K and no interactions were applied between periodic images in a cubic system with cell length 39 Å. A timestep of 0.5 fs with sampling step of 1 ps was chosen and full molecular motion was allowed throughout the simulation. The collective variable along which the metadynamics bias was accumulated measured the distance between the center of mass of the fully flexible **CC3** and the sulfur atom of the SF<sub>6</sub>. Gaussian hills with a width of 0.15 nm and an initial height of 1.2 kJ mol<sup>-1</sup> were added every 500 MD steps and the so-called well-tempered factor was set equal to 10. The free energy surface was calculated using the ‘sum\_hills’ utility of PLUMED2 with the minimum shifted to zero. An additional well-tempered metadynamics simulation using two collective variables (the distance and a torsion angle) was performed to analyse the mechanism further, see SI for further details.

**Breakthrough experiments:** Breakthrough curves were measured for a fixed bed of **CC3 $\alpha$**  or zeolite 13X at 298 K using a 90:10 (v/v) N<sub>2</sub>/SF<sub>6</sub> gas mixture. The breakthrough curves were measured using an automated breakthrough analyser (manufactured by Hiden Isochema, Warrington, U.K.).

**CC3 $\alpha$**  was made into small pellets (500–700  $\mu\text{m}$ ), which were packed into an adsorption bed for the breakthrough experiment. The materials were activated *in situ* by heating to appropriate activation temperatures and flowing helium through the column. Desorption of N<sub>2</sub>/SF<sub>6</sub> was performed by flowing helium through the bed at the same flow rate as the breakthrough experiment. The effluents were measured by an in-line mass spectrometer. Further details are in the SI.

## RESULTS AND DISCUSSION

Gas adsorption analyses revealed that all four cages were porous to SF<sub>6</sub>, but with marked differences in terms of adsorption capacities that relate to their structures (Fig. 2a–f). It is interesting that SF<sub>6</sub> is adsorbed by the smaller cages at all: from a simple static representation of their crystal structures, SF<sub>6</sub> would not be expected to be able to diffuse through the pore channels of **CC2 $\alpha$** , **CC3 $\alpha$**  and **CC13 $\beta$** . However, these organic crystals are somewhat flexible.<sup>52</sup> They are comprised of discrete molecules held together by weak intermolecular dispersion forces, rather than covalently bonded frameworks, and this has been shown previously to allow “porosity without pores”.<sup>53–55</sup> Hence **CC2 $\alpha$** , **CC3 $\alpha$**  and **CC13 $\beta$**  can adsorb SF<sub>6</sub>, despite the fact that this gas is larger than the static window diameter in the cages. The kinetic diameter of SF<sub>6</sub> is 5.5 Å,<sup>56</sup> and thus one might not expect it to diffuse into the smaller imine cages (**CC2**, **CC3**, **CC13**) since their window diameters are  $\sim 3.6$  Å.<sup>52</sup> Indeed, previous unbiased MD simulations for **CC3 $\alpha$**  demonstrated that SF<sub>6</sub> did not escape the cage cavity in which it was originally positioned over a 10 ns simulation using a forcefield tailored to describe the flexibility in imine cages.<sup>52</sup> Hence, to analyse the SF<sub>6</sub> diffusion mechanism for these smaller cages and to calculate the energetic barrier to this event, we carried out well-tempered metadynamics simulations of SF<sub>6</sub> and a single **CC3** molecule (see Supporting Information for full simulation details). To understand the diffusion mechanism, we can think of the SF<sub>6</sub> molecule as two connected triangular faces, rather than a sphere that describes the widest possible diameter. As can be seen in Figure 3 and Movie S1, SF<sub>6</sub> exits the cage by first aligning its outermost triangular face with the triangular cage window. There is then a rotation of  $\sim 60^\circ$  (Fig. 3a–d) such that the second face can align with the cage window and thus pass through. The barrier to the SF<sub>6</sub> diffusion through the flexible cage window is calculated to be at most 40 kJ mol<sup>-1</sup>, and the configurations near the saddle point have the center of the SF<sub>6</sub> traversing the window. While crystal packing effects would likely influence this barrier to a small extent, it is of similar magnitude to that previously calculated for the allowed *para*-xylene diffusion in the same host system.<sup>37</sup> It is therefore reasonable that the SF<sub>6</sub> diffuses, albeit slowly, in this system. A comparison of a single empty **CC3** window diameter distribution with the measured window diameter during the SF<sub>6</sub> passage (Fig. 3e) reveals the cooperative character of the mechanism. Clearly, the cage window size increases when the SF<sub>6</sub> is inside the window.

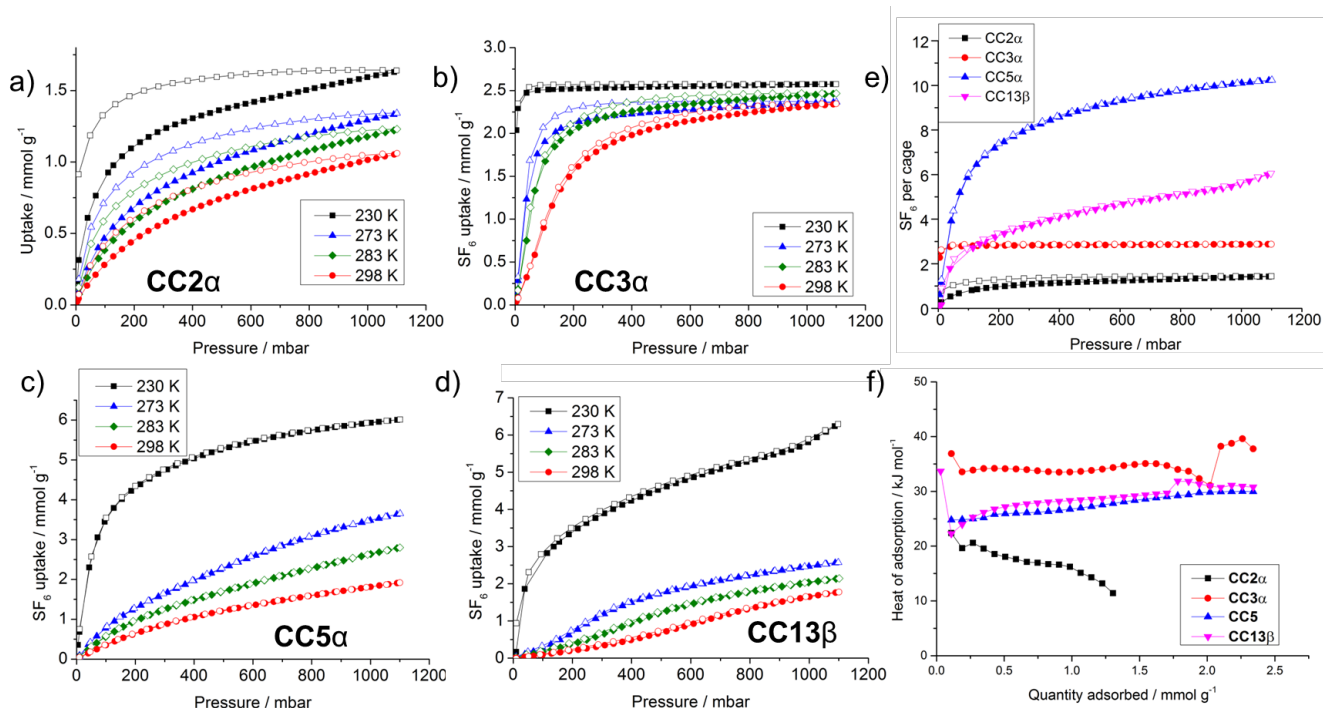


**Figure 2.** Gas sorption isotherms for the uptake of  $\text{SF}_6$  in the various cages; adsorption curves shown as filled symbols, desorption curves as unfilled symbols. a) **CC2 $\alpha$** , b) **CC3 $\alpha$** , c) **CC5 $\alpha$** , and d) **CC13 $\beta$** . e) This plot shows the uptake expressed in terms of the number of  $\text{SF}_6$  molecules per cage molecule at 230 K. f) Heat of adsorption of  $\text{SF}_6$  for the various cages.

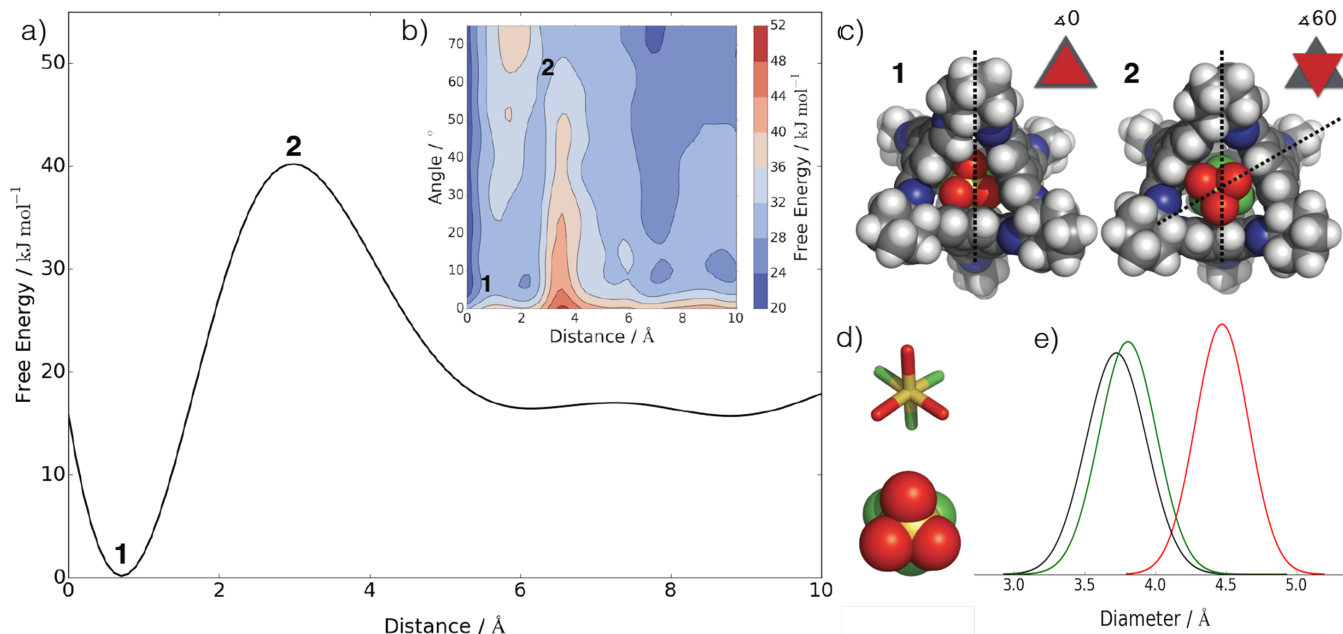


**Figure 3.** a) The free energy surface for a single  $\text{SF}_6$  molecule diffusing through the window of a single **CC3** cage as a function of the distance between the centers of mass of **CC3** and  $\text{SF}_6$ . b) The 2D free energy as a function of the distance used for (a) and the angle of rotation as shown in part (c). c) **CC3** and  $\text{SF}_6$  configurations corresponding to the positions marked **1** (left) and **2** (right) on the plots. Structure **1** corresponds to the global minimum orientation with  $\text{SF}_6$  in the **CC3** cavity and structure **2** represents the structure at highest point of the free energy surface, when  $\text{SF}_6$  is placed exactly in the center of the window. The angle used for the y-axis in panel (b) is indicated on these configurations. This angle is small when the  $\text{SF}_6$  begins to escape from the cage and increases as the  $\text{SF}_6$  reaches position **2**. d) Stick and spacefill representations of the  $\text{SF}_6$  molecule. The three fluorine atoms that diffuse through the window first are colored red. e) Comparison of the pore envelope of the **CC3** window, for an empty cage (black), for **CC3** with  $\text{SF}_6$  occupying the cage cavity (green) and for cage where  $\text{SF}_6$  is positioned in the window (red).



**CC3a** shows the highest affinity for SF<sub>6</sub> of the four cages tested, and a steep type I isotherm that saturates at low pressures (Fig. 2b). This is manifested in the highest heat of adsorption of ~35–40 kJ mol<sup>-1</sup> (Fig. 2f). The saturation uptake corresponds to around 2.9 SF<sub>6</sub> molecules per **CC3** cage (Fig. 2e). This is consistent with one SF<sub>6</sub> molecule in the internal cage cavity, plus one SF<sub>6</sub> molecule shared in each of the four window-window sites surrounding every cage, equating to a maximum theoretical loading of 3 SF<sub>6</sub> molecules per **CC3** cage. **CC2a** shows the lowest SF<sub>6</sub> uptake and the lowest heat of adsorption (Figs. 2a, 2f). The 1D pore channels in **CC2a**,<sup>33</sup> which run between the hexagonally-arrayed cages, are wide enough to accommodate SF<sub>6</sub>. The uptake of 1.4 SF<sub>6</sub> molecules per cage (Fig. 2e) confirms that these 1D channels must be at least partially occupied. **CC5a** displays the highest SF<sub>6</sub> adsorption capacity, of 10.2 SF<sub>6</sub> per cage, in line with its larger internal void size and its higher surface area and pore volume.<sup>41</sup> However, the heat of adsorption is much lower than for **CC3a**, and hence **CC5a** adsorbs less SF<sub>6</sub> at lower pressures. **CC13b** gives a lower heat of adsorption than **CC3a**, despite having a similar pore structure. The difference between the high temperature (298 K) and low temperature (230 K) SF<sub>6</sub> uptakes for **CC13b** is significant. At 230 K, **CC13b** adsorbs around 6 SF<sub>6</sub> molecules per cage – that is, twice as much gas as **CC3a**. This can be rationalized only if the SF<sub>6</sub> molecules are located in the intercage sites, of which there are three per **CC13** (Fig. 1b; blue nodes), as well as in the cage cavities and the window-window sites. While these intercage sites were shown previously to be accessible to nitrogen,<sup>31</sup> the size of the nodes relative to SF<sub>6</sub> suggested to us that significant rearrangement would be required to accommodate this larger gas. To explore this, the adsorption of SF<sub>6</sub> in **CC13b** was monitored by PXRD (Fig. 4). The PXRD pattern changes significantly as the structure is loaded with SF<sub>6</sub>, losing intensity in the high angle range. This is consistent with the preservation of the long-range packing of the cage modules, but a more disordered local structure, which could allow the large SF<sub>6</sub> guest to diffuse through the crystal. This re-organization of the **CC13** allows the incorporation of such a large quantity of SF<sub>6</sub> (6 per cage), which cannot not be rationalized by the original empty structure. It is remarkable that the crystallinity is restored completely to its initial state after removal of the SF<sub>6</sub>, even after multiple cycles (Fig. S1). This behavior is allowed by the relatively weak dispersion forces between the cages, which enable reorganization in response to guests.

The SF<sub>6</sub> isotherms for **CC3a** suggested excellent potential for SF<sub>6</sub> separation from nitrogen, and therefore the nitrogen isotherms were measured at equivalent temperatures (Fig. S2) to allow the calculation of ideal adsorbed solution theory (IAST) predicted selectivity (Figs. 5, and S3).<sup>57</sup> The industrially relevant composition for separation of an SF<sub>6</sub>/N<sub>2</sub> mixture is SF<sub>6</sub>:N<sub>2</sub> = 10%:90%.<sup>6,12</sup> At 1 bar pressure **CC3a** gives a selectivity of 178 at 273 K, and 74 at 298 K). This surpasses the most promising candidate material previously reported, UiO-66-Zr (selectivity = 74, at 1 bar, 293 K)<sup>58</sup> and other similar framework materials such as Zn-MOF-74 (selectivity = 46, at 1 bar, 298 K),<sup>6</sup> Ca-A zeolite (28 at 1 bar, 298 K),<sup>13</sup> and zeolite-13X (44 at 1 bar, 298 K).<sup>12</sup> The total capacity of **CC3a** for SF<sub>6</sub> is higher than many of the frameworks reported (e.g., UiO-66-Zr is ~1.5 mmol, at 293 K and 1 bar), but lower than the highest (Mg-MOF-74 = 6.42 mmol/g at 1 bar, 298 K).

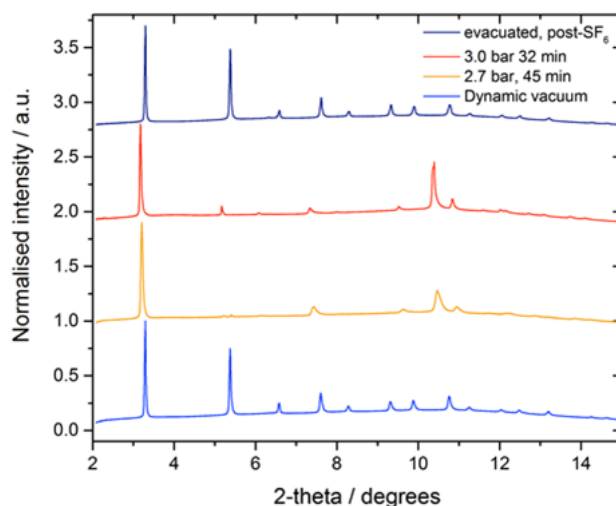


**Figure 4.** Powder X-ray diffraction data for *in situ* SF<sub>6</sub> loading of **CC13b** at 230 K. Under excess pressures of SF<sub>6</sub>, the **CC13b** structure becomes more disordered at short range, indicated by loss of high angle diffraction intensity. The original profile is totally regained after guest removal by vacuum.

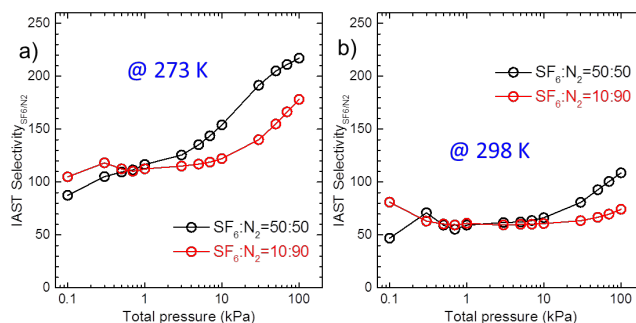


**Figure 5.** IAST selectivity plots for SF<sub>6</sub> over N<sub>2</sub> for **CC3a** at SF<sub>6</sub>:N<sub>2</sub> ratios of 50:50 and 10:90 at a) 273 K and b) 298 K.

A crystallographic study allowed for the location of SF<sub>6</sub> in **CC3a** to be accurately determined (Figs. 6, and S4). Well-ordered SF<sub>6</sub> molecules were located, with full site occupancies, in the intrinsic **CC3** cavities (Fig S4). **CC3** provides an ideal fit for SF<sub>6</sub> in terms of both size and geometry of the cage cavity (Fig. 6), which explains the high heat of adsorption that we observe. The ordering of SF<sub>6</sub> molecules in the **CC3** cavities transforms the crystallographic symmetry from *F*<sub>4</sub>32, as determined for the empty **CC3a** host, to *P*1, but this does not alter the crystal packing of the **CC3** molecules.

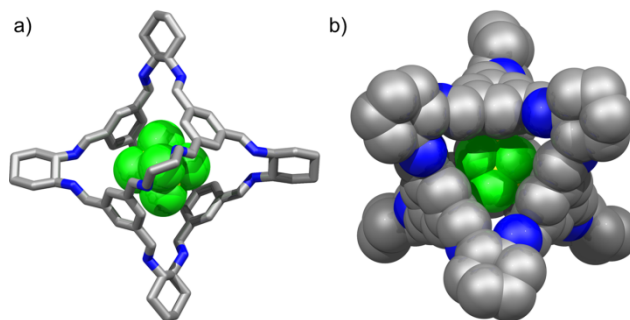


**Figure 6.** (a) Resolved position of SF<sub>6</sub> in the **CC3** cavity determined from the single crystal structure; (b) space filling representation as viewed through a cage window.

IAST calculations are useful to suggest selectivity in a separation of two or more gases for an adsorptive separation process, but IAST does not accurately represent a gas mixture flowing through a packed bed of material.<sup>58</sup> In particular, IAST calculations say little about separation kinetics since the calculations are derived from single-component gas sorption isotherms that are collected at thermodynamic equilibrium. Therefore, breakthrough experiments were carried out to establish the practical potential of **CC3 $\alpha$**  for N<sub>2</sub>/SF<sub>6</sub> separations, and in particular to demonstrate that the SF<sub>6</sub> diffusion kinetics are sufficiently fast for real separations. All breakthrough experiments were performed at 298 K with a 90:10 (v/v) N<sub>2</sub>/SF<sub>6</sub> mixture. The breakthrough curves and desorption curves for N<sub>2</sub> and SF<sub>6</sub> flowing through a bed of **CC3 $\alpha$**  are shown in Figure 7. Nitrogen breaks through the column within 1 minute, whereas SF<sub>6</sub> does not start to break through until after 6.5 minutes and does not completely break through until approximately 20 minutes. The large difference in breakthrough time between N<sub>2</sub> and SF<sub>6</sub> reflects the much higher affinity of **CC3 $\alpha$**  towards SF<sub>6</sub>. The breakthrough curve for N<sub>2</sub> shows the characteristic ‘roll-up’ as the concentration at the outlet is temporarily higher than at the inlet as the SF<sub>6</sub> is preferentially adsorbed and displaces the N<sub>2</sub>. The desorption was performed by flowing helium through the column under the same conditions as for breakthrough. N<sub>2</sub> is desorbed quickly from the column, with 97 % of the gas being desorbed within the first minute. As expected, SF<sub>6</sub> is desorbed more slowly, with full desorption taking about 20 minutes, approximately the same time as for full breakthrough.

Breakthrough and desorption curves for **CC3 $\alpha$**  and zeolite 13X at three different gas flow rates are compared in Figures S5 and S6. In each case, the desorption of SF<sub>6</sub> from **CC3** takes approximately the same time as the full breakthrough. However, for zeolite 13X with a 25 ml minute<sup>-1</sup> flow rate, SF<sub>6</sub> desorption takes twice as long as it does to breakthrough (Figure S6). The more rapid desorption efficiency of **CC3 $\alpha$**  therefore gives it a potential advantage over zeolite 13X as a material for N<sub>2</sub>/SF<sub>6</sub> separation.<sup>59</sup>

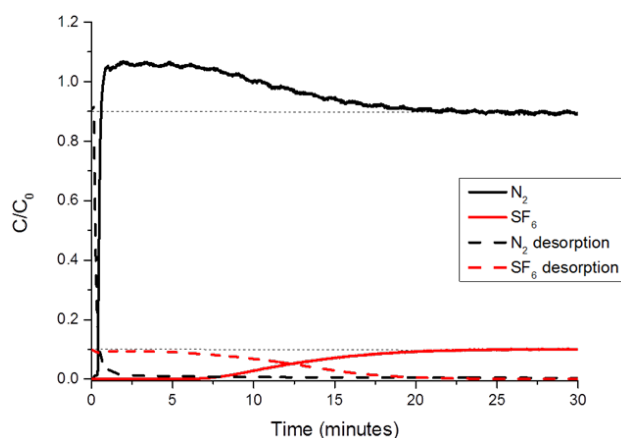


**Figure 7.** N<sub>2</sub>/SF<sub>6</sub> (90:10) breakthrough curve for **CC3 $\alpha$**  at 298 K. The total flow rate was 25 ml min<sup>-1</sup> and the pressure was 1 bar. Desorption was performed by flowing helium through the bed at the same flow rate and pressure.

## SUMMARY

Intrinsically porous molecules, as opposed to framework or network materials, have been investigated for SF<sub>6</sub> uptake separation. Despite the pore limiting diameters in **CC3** being considerably narrower<sup>36,52</sup> than the 11 Å recommended as the optimum pore size by simulation,<sup>60</sup> this cage shows unprecedented selectivity for SF<sub>6</sub> over N<sub>2</sub>. Our simulations suggest this may be a result of the flexibility of the **CC3** molecular crystal, which allows SF<sub>6</sub> to diffuse by cooperative effects, before the structure relaxes back to produce a closer, near-ideal interaction with the SF<sub>6</sub> guest. This hypothesis is further supported by research reported by Camp and Scholl while this manuscript was being written.<sup>61</sup> In that study, transition state theory methods were used to simulate the diffusion of various gases in **CC3**, and it was found for SF<sub>6</sub> that no diffusion would be expected in a static system, while diffusion should be possible if the flexibility of the host is taken into account. The IAST selectivity of **CC3** for an industrially relevant mixture of 10:90 SF<sub>6</sub>:N<sub>2</sub> at 298 K and 1 bar is higher than other reported materials. Breakthrough experiments confirmed that **CC3** is effective for separation of N<sub>2</sub> and SF<sub>6</sub>. Also, desorption curves show that SF<sub>6</sub> is more efficiently desorbed from **CC3** than from zeolite 13X. Flexibility in MOFs has been found to provide higher gas capacities.<sup>62</sup> Similarly, the flexibility of molecular crystals, such as **CC3**, allows for a stronger gas binding with SF<sub>6</sub>, which gives these materials potential for practical gas separations under flow.

## ASSOCIATED CONTENT

Crystallographic details, analysis equipment and conditions, and further characterization details. This material is available free of charge via the Internet at <http://pubs.acs.org>.

## AUTHOR INFORMATION

### Corresponding Author

\* [aicooper@liv.ac.uk](mailto:aicooper@liv.ac.uk)

## ACKNOWLEDGMENT

We thank the Engineering and Physical Sciences Research Council (EP/H000925/1 and EP/K018396/1) and the European Research Council under FP7 (RobOT, ERC grant agreement no. 321156). T. H. and K. E. J. are Royal Society University Research Fellows. We thank the STFC for access to Diamond Light Source and the staff at beamlines I19 (MT8728) and I11 (EE9282), and Drs. C. Murray and A. Baker for help with gas cell experiments.

## ABBREVIATIONS

**CCX**, referring to a ‘covalent cage’ of a series published by the Cooper group, X being the order of publishing, see cited references. PXRD, powder x-ray diffraction. BET, Brunauer–Emmett–Teller. PSD, position sensitive detector. IAST, ideal adsorbed solution theory.

## REFERENCES

- (1) Ravishankara, A. R.; Solomon, S.; Turnipseed, A. A.; Warren, R. F. *Science* **1993**, 259, 194.
- (2) Fang, X.; Hu, X.; Janssens-Maenhout, G.; Wu, J.; Han, J.; Su, S.; Zhang, J.; Hu, J. *Environ. Sci. Technol.* **2013**, 47, 3848.
- (3) Solomon, S.; Qin, D.; Manning, M. Technical Summary; Cambridge Univ Press: New York, 2007.

- (4) Christophorou, L. G.; Vanbrunt, R. J. *IEEE T. Dielect. El. In.* **1995**, 2, 952.
- (5) Senkovska, I.; Barea, E.; Rodriguez Navarro, J. A.; Kaskel, S. *Micropor. Mesopor. Mat.* **2012**, 156, 115.
- (6) Kim, M.-B.; Lee, S.-J.; Lee, C. Y.; Bae, Y.-S. *Micropor. Mesopor. Mat.* **2014**, 190, 356.
- (7) Yang, R. T. In *Adsorbents: Fundamentals and Applications*; John Wiley & Sons, Inc, Hoboken, New Jersey.: **2003**, p 17.
- (8) Cao, D. V.; Sircar, S. *Adsorption* **2001**, 7, 73.
- (9) Cho, W.-S.; Lee, K.-H.; Chang, H.-J.; Huh, W.; Kwon, H.-H. *Korean J. Chem. Eng.* **2011**, 28, 2196.
- (10) Chiang, Y.-C.; Wu, P.-Y. *J. Hazard. Mater.* **2010**, 178, 729.
- (11) Cao, D. V.; Sircar, S. *Ind. Eng. Chem. Res.* **2001**, 40, 156.
- (12) Murase, H.; Imai, T.; Inohara, T.; Toyoda, M. *IEEE T. Dielect. El. In.* **2004**, 11, 166.
- (13) Toyoda, M.; Murase, H.; Imai, T.; Naotsuka, H.; Kobayashi, A.; Takano, K.; Ohkuma, K. *IEEE T. Power Deliver.* **2003**, 18, 442.
- (14) Bandosz, T. J.; Jagiello, J.; Schwarz, J. A. *J. Chem. Eng. Data* **1996**, 41, 880.
- (15) Holst, J. R.; Trewin, A.; Cooper, A. I. *Nat. Chem.* **2010**, 2, 915.
- (16) Tian, J.; Thallapally, P. K.; McGrail, B. P. *CrystEngComm* **2012**, 14, 1909.
- (17) Zhang, G.; Mastalerz, M. *Chem. Soc. Rev.* **2014**, 43, 1934.
- (18) Slater, A. G.; Cooper, A. I. *Science* **2015**, 348, 988.
- (19) Jin, Y. H.; Wang, Q.; Taynton, P.; Zhang, W. *Accounts Chem. Res.* **2014**, 47, 1575.
- (20) Ding, H.; Yang, Y.; Li, B.; Pan, F.; Zhu, G.; Zeller, M.; Yuan, D.; Wang, C. *Chem. Commun.* **2015**, 51, 1976.
- (21) Wang, Q.; Zhang, C. X.; Noll, B. C.; Long, H.; Jin, Y. H.; Zhang, W. *Angew. Chem. Int. Ed.* **2014**, 53, 10663.
- (22) Zhang, C.; Chen, C. F. *J. Org. Chem.* **2007**, 72, 9339.
- (23) Zhang, C.; Wang, Z.; Tan, L.; Zhai, T.-L.; Wang, S.; Tan, B.; Zheng, Y.-S.; Yang, X.-L.; Xu, H.-B. *Angew. Chem. Int. Ed.* **2015**, 54, 9244.
- (24) Evans, J. D.; Sumby, C. J.; Doonan, C. J. *Chem. Lett.* **2015**, 44, 582.
- (25) Mastalerz, M.; Oppel, I. M. *Angew. Chem. Int. Ed.* **2012**, 51, 5252.
- (26) Schneider, M. W.; Hauswald, H. J. S.; Stoll, R.; Mastalerz, M. *Chem. Commun.* **2012**, 48, 9861.
- (27) Riddell, I. A.; Smulders, M. M. J.; Clegg, J. K.; Nitschke, J. R. *Chem. Commun.* **2011**, 47, 457.
- (28) Mastalerz, M. *Angew. Chem. Int. Ed.* **2010**, 49, 5042.
- (29) Avellaneda, A.; Valente, P.; Burgun, A.; Evans, J. D.; Markwell-Heys, A. W.; Rankine, D.; Nielsen, D. J.; Hill, M. R.; Sumby, C. J.; Doonan, C. J. *Angew. Chem. Int. Ed.* **2013**, 52, 3746.
- (30) Zhang, G.; Presly, O.; White, F.; Oppel, I. M.; Mastalerz, M. *Angew. Chem. Int. Ed.* **2014**, 53, 1516.
- (31) Hasell, T.; Culshaw, J. L.; Chong, S. Y.; Schmidtman, M.; Little, M. A.; Jelfs, K. E.; Pyzer-Knapp, E. O.; Shepherd, H.; Adams, D. J.; Day, G. M.; Cooper, A. I. *J. Am. Chem. Soc.* **2014**, 136, 1438.
- (32) Mitra, T.; Wu, X.; Clowes, R.; Jones, J. T. A.; Jelfs, K. E.; Adams, D. J.; Trewin, A.; Bacsa, J.; Steiner, A.; Cooper, A. I. *Chem. Eur. J.* **2011**, 17, 10235.
- (33) Tozawa, T.; Jones, J. T. A.; Swamy, S. I.; Jiang, S.; Adams, D. J.; Shakespeare, S.; Clowes, R.; Bradshaw, D.; Hasell, T.; Chong, S. Y.; Tang, C.; Thompson, S.; Parker, J.; Trewin, A.; Bacsa, J.; Slawin, A. M. Z.; Steiner, A.; Cooper, A. I. *Nat. Mater.* **2009**, 8, 973.
- (34) Jones, J. T. A.; Holden, D.; Mitra, T.; Hasell, T.; Adams, D. J.; Jelfs, K. E.; Trewin, A.; Willock, D. J.; Day, G. M.; Bacsa, J.; Steiner, A.; Cooper, A. I. *Angew. Chem. Int. Ed.* **2011**, 50, 749.
- (35) Little, M. A.; Chong, S. Y.; Schmidtman, M.; Hasell, T.; Cooper, A. I. *Chem. Commun.* **2014**, 50, 9465.
- (36) Chen, L.; Reiss, P. S.; Chong, S. Y.; Holden, D.; Jelfs, K. E.; Hasell, T.; Little, M. A.; Kewley, A.; Briggs, M. E.; Stephenson, A.; Thomas, K. M.; Armstrong, J. A.; Bell, J.; Busto, J.; Noel, R.; Liu, J.; Strachan, D. M.; Thallapally, P. K.; Cooper, A. I. *Nat. Mater.* **2014**, 13, 954.
- (37) Mitra, T.; Jelfs, K. E.; Schmidtman, M.; Ahmed, A.; Chong, S. Y.; Adams, D. J.; Cooper, A. I. *Nat. Chem.* **2013**, 5, 276.
- (38) Kewley, A.; Stephenson, A.; Chen, L. J.; Briggs, M. E.; Hasell, T.; Cooper, A. I. *Chem. Mater.* **2015**, 27, 3207.
- (39) Zhang, J.-H.; Xie, S.-M.; Chen, L.; Wang, B.-J.; He, P.-G.; Yuan, L.-M. *Anal. Chem.* **2015**, 87, 7817.
- (40) Hasell, T.; Chong, S. Y.; Jelfs, K. E.; Adams, D. J.; Cooper, A. I. *J. Am. Chem. Soc.* **2012**, 134, 588.
- (41) Jones, J. T. A.; Hasell, T.; Wu, X.; Bacsa, J.; Jelfs, K. E.; Schmidtman, M.; Chong, S. Y.; Adams, D. J.; Trewin, A.; Schiffman, F.; Cora, F.; Slater, B.; Steiner, A.; Day, G. M.; Cooper, A. I. *Nature* **2011**, 474, 367.
- (42) Nowell, H.; Barnett, S. A.; Christensen, K. E.; Teat, S. J.; Allan, D. R. *J. Synch. Rad.* **2012**, 19, 435.
- (43) Sheldrick, G. M. *SADABS. University of Göttingen, Germany* **2008**.
- (44) Sheldrick, G. M. *Acta Cryst. Sect. A* **2008**, 64, 112.
- (45) Dolomanov, O. V.; Bourhis, L. J.; Gildea, R. J.; Howard, J. A. K.; Puschmann, H. *J. Appl. Cryst.* **2009**, 42, 339.
- (46) Parker, J. E.; Potter, J.; Thompson, S. P.; Lennie, A. R.; Tang, C. C.; *Mater. Sci. Forum* **2012**, 706-709, 1707-1712.
- (47) Smith, W.; Yong, C. W.; Rodger, P. M. *Mol. Simul.* **2002**, 28, 385-471.
- (48) Tribello, B.; Bonomi, Branduardi, Camilloni, and Bussi, *Comput. Phys. Commun.* **2014**, 185, 604.
- (49) Jorgensen, W. L.; Maxwell, D. S. & Tirado-Rives, J. *J. Am. Chem. Soc.* **1996**, 118, 11225-11236.
- (50) Hockney, R. W. *Methods Comput. Phys.* **1970**, 9, 135.
- (51) Hoover, W. G. *Phys. Rev. A* **1985**, 31, 1695.
- (52) Holden, D.; Jelfs, K. E.; Trewin, A.; Willock, D. J.; Haranczyk, M.; Cooper, A. I. *J. Phys. Chem. C* **2014**, 118, 12734.
- (53) Barbour, L. J. *Chem. Commun.* **2006**, 1163.
- (54) Dobrzanska, L.; Lloyd, G. O.; Raubenheimer, H. G.; Barbour, L. J.; *J. Am. Chem. Soc.* **2006**, 128, 698.
- (55) Herbert, S. A.; Janiak, A.; Thallapally, P. K.; Atwood, J. L.; Barbour, L. J. *Chem. Commun.* **2014**, 50, 15509.
- (56) D. W. B. In *Molecular Sieve Zeolites-I*; American Chemical Society: 1974; Vol. 101, p 1.
- (57) Myers, A. L.; Prausnitz, J. M. *Aiche J.* **1965**, 11, 121.
- (58) Kim, M.-B.; Yoon, T.-U.; Hong, D.-Y.; Kim, S.-Y.; Lee, S.-J.; Kim, S.-I.; Lee, S.-K.; Chang, J.-S.; Bae, Y.-S. *Chem. Eng. J.* **2015**, 276, 315.
- (59) Kim, P.-J.; You, Y.-W.; Park, H.; Chang, J.-S.; Bae, Y.-S.; Lee, C.-H.; Suh, J.-K. *Chem. Eng. J.* **2015**, 262, 683.
- (60) Builes, S.; Roussel, T.; Vega, L. F. *Aiche J.* **2011**, 57, 962.
- (61) Camp, J. S.; Sholl, D. S. *J. Phys. Chem. C* **2015**.
- (62) Mason, J. A.; Oktawiec, J.; Taylor, M. K.; Hudson, M. R.; Rodriguez, J.; Bachman, J. E.; Gonzalez, M. I.; Cervellino, A.; Guagliardi, A.; Brown, C. M.; Llewellyn, P. L.; Masciocchi, N.; Long, J. R. *Nature* **2015**, 527, 357-361.



